CMLS, Cell. Mol. Life Sci. 61 (2004) 2060–2070
1420-682X/04/162060-11
DOI 10.1007/s00018-004-4074-3

CMLS Cellular and Molecular Life Sciences

Research Article

Differential effects of monastrol in two human cell lines

I. Leizerman [a], R. Avunie-Masala [a], M. Elkabets [a], A. Fich [b] and L. Gheber [a,b,*]

[a] Department of Clinical Biochemistry, Ben-Gurion University of the Negev, P. O. Box 653, Beer-Sheva 84105 (Israel), Fax: +972 8 6281361, e-mail: lgheber@bgumail.bgu.ac.il
[b] Department of Gastroenterology, Ben-Gurion University of the Negev and Soroka University Medical Center, Beer-Sheva (Israel)

Received 18 February 2004; received after revision 30 May 2004; accepted 16 June 2004

Abstract. The kinesin-related protein HsEg5 plays essential roles in mitotic spindle dynamics. Although inhibition of HsEg5 has been suggested as an aid in cancer treatment, the effects of such inhibition on human cells have not been characterized. Here we studied the effects of monastrol, an allosteric HsEg5 inhibitor, on AGS and HT29 cell lines and compared them to those of taxol. While both cell lines were similarly sensitive to taxol, AGS cells were more sensitive to monastrol. The differences in sensitivity were determined by the degree of inhibitory effect on cell proliferation, reversibility of monastrol-induced G2/M arrest, intracellular phenotypes and induction of apoptosis. In both cell lines, monastrol-induced apoptosis was accompanied by mitochondrial membrane depolarization and poly-ADP-ribose polymerase 1 cleavage. In AGS, but not HT29 cells, monastrol-induced apoptosis involved a prominent cleavage of procaspases 8 and 3. While in AGS cells, monastrol induced the formation of symmetric microtubule asters only, in HT29 cells, asymmetric asters were also formed, which may be related to specific HsEg5 functions in HT29 cells.

Key words. Monastrol; HsEg5; mitotic spindle; microtubule; taxol; apoptosis.

Mitotic cell division is an essential process by which duplicated genomic information is transmitted from mother to daughter cells. Incorrect chromosome segregation has severe consequences, including cell death, genetic diseases and cancer. This essential process is mediated by the mitotic spindle, a highly dynamic, microtubule-based structure, which undergoes a distinct set of morphological changes. Many of these changes have been attributed to the action of molecular motors which use ATP hydrolysis to unidirectionally move along microtubules. Members of the cytoplasmic dynein and the kinesin superfamilies have been implicated in mitotic movement in eukaryotes [reviewed in refs 1–4].

Numerous studies have demonstrated that drugs which disrupt mitotic spindles and inhibit mitosis can be effective in inhibiting the proliferation of cancer cells [5, 6]. These antimitotic agents have also been shown to kinetically inhibit the normal dynamics of microtubules. For example, colchicine [7] binds to soluble tubulin and is then incorporated into a growing microtubule, and vinblastine [7] binds to microtubule ends thereby suppressing microtubule dynamics. At high concentrations, both colchicine and vinblastine cause the loss of cellular microtubules. Paclitaxel (more commonly known as taxol) and related taxanes also inhibit microtubule dynamics. At high concentrations, these agents increase the polymerized tubulin in a cell, thereby causing the formation of thick microtubule bundles [8]. However, a serious drawback of anticancer agents that alter microtubule dynamics is that they interfere not only with mitosis, but also with other intracellular functions that require microtubules, such as vesicle trafficking, thereby affecting nonmitotic cells.

* Corresponding author.

Monastrol is a cell-permeable molecule that inhibits the mitotic machinery without targeting microtubules [9], and may be a potentially powerful tool for inhibiting cancer cell growth. After short exposure, monastrol arrests cells in mitosis with monoastral spindles comprised of a radial array of microtubules surrounded by a ring of chromosomes. Monastrol does not affect microtubules in interphase cells, microtubule polymerization in vitro or lysosome and Golgi apparatus intracellular distribution [9]. Biochemical studies have shown that monastrol is an allosteric inhibitor of kinesin-related proteins from the BimC family [9–13].

Members of the BimC family have been identified in a large number of eukaryotes [14–20], including humans [21], and have been implicated in conserved and essential mitotic functions [22, 23]. These proteins are conserved in the amino acid sequence of the motor (force-producing) domain and are believed to perform their mitotic functions by cross-linking antiparallel microtubules and moving toward the microtubule 'plus' ends [24]. In human cells, elimination of the function of the BimC kinesin HsEg5 interferes with bipolar spindle dynamics. After HsEg5 function has been inhibited, cells are blocked in mitosis and contain monoastral microtubule arrays [13, 21]. Since the long-term effect of HsEg5 function inhibition on human cells has not been characterized, the anticancer potential of such treatment has not been evaluated.

When mitotic arrest is imposed for prolonged periods, cells often undergo programmed death, known as apoptosis. Apoptosis is associated with morphological changes, including membrane blebbing, cellular shrinkage, chromatin condensation and detachment from the extracellular matrix [25]. It is also associated with biochemical changes, including activation of a cascade of proteases such as the caspases and endonucleases, cleavage of poly-ADP-ribose polymerase 1 (PARP-1), and eventually fragmentation of genomic DNA [26, 27]. Caspase 3 is considered the first caspase involved in the execution phase of apoptosis and is activated by the proteins involved in the initiating phase (i.e. caspase 8, and cytochrome C). One of the downstream targets of caspase 3 is PARP-1, which promotes DNA repair [28]. Therefore, inactivation of PARP-1 by caspase 3 cleavage prevents DNA repair, which results in internucleosomal DNA fragmentation. Antimicrotubule drugs that induce mitotic arrest, such as taxol, often induce cellular apoptosis [29, 30]. Taxol was shown to induce apoptosis via mitochondrial depolarization [31, 32], activating upstream caspase 8 [31, 32], downstream caspase 3 [32, 33] and PARP-1 cleavage [34, 35]. Since monastrol induces mitotic arrest without affecting microtubule dynamics, whether prolonged monastrol-induced mitotic arrest also leads to apoptosis, and if monastrol and taxol trigger similar apoptotic pathways is not clear.

Short-term monastrol-induced mitotic arrest has been demonstrated in *Xenopus laevis* cell extracts, in mammalian PtK1 and PtK2 cells from rat kangaroo kidney epithelium [10, 36], BS-C-1 cells from monkey kidney [10] as well as in a human HeLa cell line from a cervical carcinoma [13]. Long-term (>20 h) effects of monastrol on human cells have not as yet been studied. Therefore, in the present study, we examined its long-term effect on cell proliferation and apoptosis in human AGS and HT29 cell lines from gastric and colon carcinomas. We compared the sensitivity of these cell lines to monastrol treatment and characterized monastrol-induced microtubule rearrangement. We also compared the effects of monastrol to those of taxol, an anticancer agent that inhibits cell proliferation and often causes G2/M cell cycle arrest.

Materials and methods

Cell culture and monastrol and taxol treatment of cells

AGS cells were grown in DMEM/F-12 (HAM) 1:1 (Beit Haemek, Israel), and HT29 cells in DMEM medium at 37 °C in a humidified atmosphere of a 5% CO_2 incubator (Tuttnauer, New York, N.Y.). Both media were supplemented with 10% fetal calf serum, 2 mM L-glutamine and 1% antibiotic-antimycotic solution containing 10 units/µl penicillin, 10 µg/µl streptomycin and 1250 units/ml nystatin (Beit Haemek, Kibbutz Beit Haemek, Israel). Unless otherwise indicated, monastrol (Tocris, Avonmount, UK) concentrations of 100 µM for AGS cells and 150 µM for HT29 cells were used, while taxol (Sigma, St. Louis, Mo.) concentrations were 10 nM or 100 nM for both cell lines. To study the reversibility of monastrol and taxol treatments, AGS and HT24 cells were treated for 24, 48 or 72 h. Then, medium containing the drug was removed and replaced with normal medium. To release HT29 from monastrol or taxol arrest, floating cells were also collected, washed three times with normal medium and plated in a new petri dish. To examine the effect of monastrol and taxol on cell proliferation, the number of viable cells was determined by trypan blue dye (Sigma) exclusion. Control experiments were performed in the presence of DMSO, a solvent of monastrol and taxol.

Immunostaining

To visualize the microtubule cytoskeleton and DNA, AGS and HT29 cells were cultured on coverslips, fixed with 4% paraformaldehyde for 30 min and permeabilized for 2 min with 0.3% Triton-X-100 in 4% paraformaldehyde. Then, the cells were washed with buffer containing 100 mM PIPES, pH 6.8, 1 mM $MgCl_2$ and 10 mM EGTA (all Sigma). All consequent washes were done with PBS containing 0.1% BSA (Sigma). Coverslips were incu-

bated for 1 h at room temperature with rat anti-tubulin YOL1/34 and then for 1 h with Alexa 488 conjugated anti-rat secondary antibody. DNA was visualized by incubation with 0.07 µg/ml DAPI for 5 min. Immunostained cells were observed with an Olympus BX51 microscope equipped with appropriate filters. Cells in interphase or mitosis were counted and categorized.

Cell cycle analysis

For cell cycle analysis, floating and adherent cells were fixed with 70% ethanol and stored at –20 °C for at least 7 days. The fixed cells were collected by centrifugation and resuspended in 0.1% Triton-X-100 and 30 µg/ml RNAse A type I-A (Sigma), at room temperature for 40 min. Nuclear DNA was stained with 15 µg propidium iodide in PBS solution and the DNA content was measured by flow cytometry (BD Biosciences, Oxford, UK). Cell proportions in sub-G0/G1, G0/G1, S and G2/M phases were analyzed using appropriate software. For each sample, 10,000 cells were scored.

JC-1 staining

Mitochondrial depolarization was examined with the cationic dye JC-1 (Molecular Probes) which exhibits potential-dependent accumulation in mitochondria. Cells were stained with 10 µg/ml JC-1, for 10 min, at 37 °C in a humidified incubator. Then, cells were washed with PBS and observed under an Olympus BX51 microscope, with a wide FITC filter set.

Acridine orange and ethidium bromide staining

To examine the appearance of early and late apoptosis, cells were stained with acridine orange and ethidium bromide, which allows us to distinguish between live, early and late apoptotic cells by detection of fragmented DNA and membrane integrity [37]. Adherent and floating cells were stained with 10 µg acridine orange and 10 µg ethidium bromide for 5 min. The cells were observed under an Olympus BX51 microscope, with a wide FITC filter.

mRNA analysis

Levels of HsEg5 and β-actin were determined by reverse-transcription PCR (RT-PCR) of total RNA extracted from AGS and HT29 cells treated with monastrol or taxol. Total RNA extraction was performed with the RNeasy mini kit (Qiagen, Hilden, Germany), with DNAse (Qiagen) treatment to ensure removal of genomic DNA. The cDNA template was prepared using half of the RNA samples, with the first-strand synthesis kit (Abgene, Epsom, UK). For quantitative real-time PCR, templates (7 µl) were diluted ninefold and mixed with primers (0.2 mM) and Thermo-Start master mix (Abgene). SYBR green I dye (Amresco, Solon, Ohio) was added to the reaction mixture. Primers for PCR amplification and product size were as follows: HsEg5 – sense: 5′-TCC CAA CAG GTA CGA CAC CAC AGA-3′; antisense: 5′- GCC TCT TCT ACA TCC ACA TCC GGA-3′; product size – 181 bp. β-Actin sense: 5′-ATG GAT GAT GAT ATC GCC GCG-3′; antisense: 5′-CTA GAA GCA TTT GCG GTG GAC GAT GGA GGG GCC-3′; product size 238 bp. Reactions were carried out in the Rotor-Gene Real-Time PCR apparatus (Corbett-Research, Mortlake, Australia). Standard cycling conditions for this instrument were used: 15 min initial enzyme activation at 95 °C, then 40 cycles at 95 °C for 15 s, annealing temperature according to the primers for 15 s and 72 °C for 15 s. The annealing temperature for HsEg5 primers was 65 °C and for β-actin primers, 60 °C. The results were analyzed by Rotor-Gene real-time analysis software. The linear phase of double-stranded DNA synthesis was reached at 20 cycles for β-actin and at 25 cycles for HsEg5. For each sample, the levels of HsEg5 were normalized to the β-actin levels (relative expression). Real-time PCR analysis was performed for three different experiments. To compare the two cell lines, in each experiment, HsEg5 relative expressions were normalized to their relative expression in AGS control samples. To visualize the amplification products we also performed PCR (Biometra, Göttingen, Germany) using the same primers and templates as for real-time PCR. Cycling conditions were as follows: 95 °C for 30 s, annealing for 30 s, 72 °C for 45 s. The number of cycles and annealing temperatures for each product were as indicated above for real-time PCR. PCR products (10 µl) were fractionated on a 2% agarose gel; DNA was visualized by ethidium bromide staining and quantified by video densitometry (ImageMaster; Amersham, Piscataway, N.J.).

Western blot analysis

Whole-cell lysates were prepared by suspending cells in 150 µl of lysis buffer [50 mM HEPES pH 7.5, 150 mM NaCl, 10% glycerol, 1% Triton-X-100, 1.5 mM $MgCl_2$, 1 mM EGTA, 20 mM phosphate, 50 mM NaF, 3 mM EDTA, 2 mM sodium orthovanadate, 1 mM mixture of protease inhibitors (Amersham, Piscataway, N.J.) and 0.2 mM DTT (Sigma)] for 10 min on ice. Lysates were centrifuged and the supernatant was collected. Aliquots of 20 µg protein were separated on 10% SDS-polyacrylamide gels and transferred onto a polyvinylidene fluoride membrane (Millipore, Billerica, Mass.). After blocking with 5% nonfat milk in PBS. (137 mM NaCl, 2.7 mM KCl, 10 mM Na_2HPO_4, 2 mM KH_2PO_4) containing 0.1% Tween-20 (PBST) and 1% BSA, the membranes were incubated with the appropriate primary and horseradish peroxidase-conjugated secondary antibodies (in PBST containing 1% BSA). We used a semi-quantitative approach to determine the degree of change in expression of the apoptotic proteins procaspase 8, 3 and PARP-1. For this purpose, Western blot films were scanned and digitized. The intensity of a rectangular area that included a band of in-

terest was determined by ImageJ software. We then performed several normalization steps. The background of each band was subtracted by measuring the intensity of the same rectangular area near the band of interest. To normalize to the total protein quantity in each sample, the band intensity of the apoptotic proteins was divided by the band intensity of β-actin in the same sample. Finally, the normalized band intensity of each protein obtained after treatment with monastrol or taxol was divided by the same protein band intensity obtained in the control experiment. This resulted in a normalized value of protein expression relative to control.

The antibodies used in this study were purchased from Santa Cruz Biotechnology (Santa Cruz, Calif.) – anti caspase 3 (1:600), Alexis Biochemicals (San Diego, Calif.) – anti caspase 8 (1:600), Biomol (Plymouth, Pa.) – anti PARP-1 (1:1500), Oncogene (Carpinteria, Calif.) – anti β-actin (1:20,000), Promega (Madison, Wisc.) – HRP-conjugated goat anti-mouse and anti-rabbit (1:20,000), Serotec (Oxford, UK) – anti-tubulin (1:1200) and Molecular Probes (Eugene, Oreg.) – Alexa 488-conjugated anti-rat (1:600).

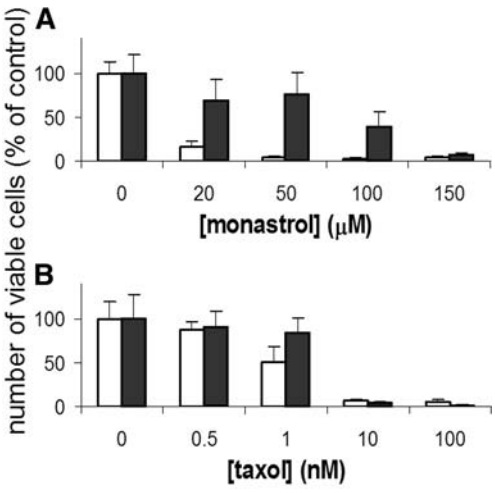

Figure 1. Effects of monastrol and taxol on cell viability. AGS cells (white columns) and HT29 cells (black columns) were incubated for 3 days with various concentrations of monastrol (*A*) and taxol (*B*). The number of viable cells (% of control) was determined by trypan blue staining. Monastrol and taxol concentrations are indicated in the abscissa. Columns and bars represent averages and SD of three to four experiments.

Results

Monastrol and taxol inhibit cell proliferation

We first characterized the long-term effect of monastrol and taxol on the viability of human cell lines. We exposed cells from AGS and HT29 cell lines to various concentrations of monastrol and taxol for 3 days, and determined the number of viable cells (fig. 1). We found that both AGS and HT29 cells responded similarly to taxol since growth of both cell lines was inhibited by 10 nM of taxol (fig. 1B). On the other hand, the two cell lines responded differently to prolonged exposure to monastrol (fig. 1A). At 50 μM, monastrol inhibited AGS cell growth, while HT29 cell growth was completely inhibited only at concentrations as high as 150 μM (fig. 1A). Similar results were also obtained after 4 days of monastrol treatment (data not shown). These results indicate that HT29 cells are less sensitive than AGS cells to monastrol. Based on this difference, 100 and 150 μM of monastrol were used to study the effects on AGS and HT25 cells, respectively. Taxol concentrations in later experiments were 10 and 100 nM for both cell lines.

Monastrol treatment for 24 h induces reversible G2/M arrest

We found that prolonged treatment with monastrol or taxol induces G2/M arrest in both AGS and HT29 cells (fig. 2). A 24-h arrest induced by monastrol was reversible in both cells lines, as the cell cycle returned to normal after removal of monastrol (fig. 2A). On the other hand, G2/M arrest induced by 24 h treatment with 10 nM taxol was irreversible in AGS cells and only partially reversible in HT29 cells (Fig. 2A). At higher taxol concentrations, such as 100 nM, G2/M arrest in both AGS and HT29 cells was irreversible (data not shown). These results indicate that although monastrol and taxol induce G2/M cell cycle arrest, both AGS and HT29 cells are less sensitive to monastrol-induced arrest than to taxol-induced arrest.

Prolonged monastrol treatment induces irreversible G2/M arrest in AGS cells

While 24 h monastrol-induced arrest of AGS cells was reversible, a 48 h arrest was not, since after removal of monastrol, the majority of cells remained in the G2/M phase of the cell cycle (fig. 2B). In addition, after 48 h of monastrol treatment of AGS cells, the number of cells containing sub-G1 DNA content increased. This may indicate that AGS cells irreversibly arrested in the G2/M phase by monastrol undergo apoptosis. Consistent with the lower sensitivity of HT29 cells to monastrol (fig. 1A), 48 h of monastrol treatment of HT29 cells resulted in partial release from arrest, with about 30% of HT29 cells in G1 phase, compared to 50% in untreated cells (fig. 2B). The difference in sensitivity between the two cell lines is specific to monastrol, since in taxol-induced arrest, about 90% of HT29 cells were in the G2/M phase and arrest was not reversible. In agreement with reports on various cell lines [38], 48 h taxol treatment of AGS cells increased the cell population with a larger than 2n DNA content, from 5 % in control cells to 15% in taxol-treated cells (data not shown). This result indicates that taxol induces polyploidy in AGS cells. In HT29 cells treated with taxol for 48 h, and in both cell lines treated with monas-

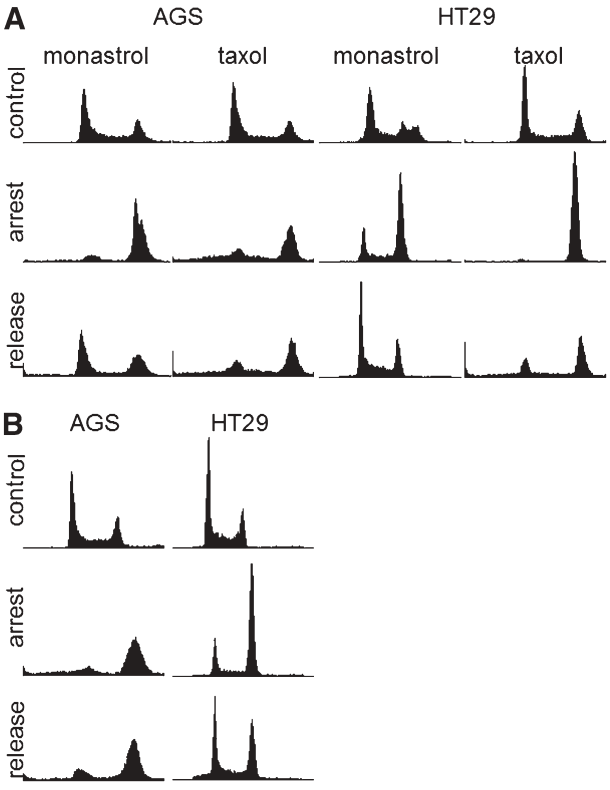

Figure 2. Effect of monastrol and taxol on cell cycle phase distribution. Cell cycle of AGS cells and HT29 cells was monitored by flow cytometry after inhibition with taxol or monastrol for 24 h (*A*) or with monastrol for 48 h (*B*) (arrest). To examine the reversibility of arrest, the cell cycle was also monitored 24 h after removal of the drug (release).

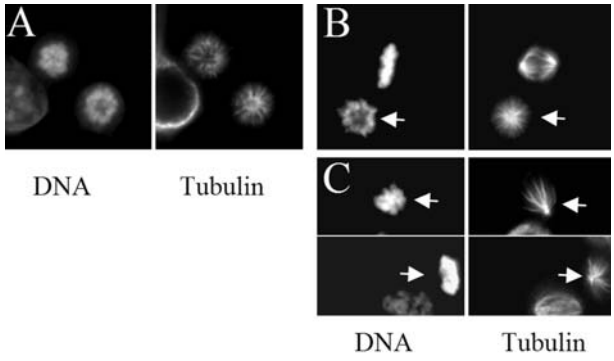

Figure 3. Effect of monastrol on intracellular microtubule arrangement. AGS (*A*) and HT29 (*B*, *C*) cells were treated with monastrol for 24 h. Representative microtubule (right panels) and DNA (left panels) structures of the same cells are shown. Symmetric asters were observed in both AGS (*A*) and HT29 (*B*) (arrow) cells. Asymmetric asters were observed only in HT29 cells (*C*) (arrow).

trol for 48 h, the increase in polyploidy was nominal (data not shown).

Differential effect of monastrol on the microtubule arrangement of AGS and HT29 cells

We examined whether the different sensitivities of AGS and HT29 cells to monastrol (figs 1, 2) could be related to differences in microtubule arrangement. We observed spindle morphologies in AGS and HT29 cells arrested with 100 µM and 150 µM monastrol, respectively, and released into normal medium. After 24 h of monastrol arrest, about 40% of the cells from both cell lines were in mitosis, as indicated by their DNA morphology and microtubule organization (fig. 3). A similar percentage of mitotic cells was also observed in HeLa cells treated with monastrol for 20 h [13]. Before removing monastrol, nearly all of the mitotic cells had monoastral spindles. Surprisingly, we found that in the two cell lines, the monastrol-induced microtubule asters were shaped differently. In AGS cells, all the asters were centered and symmetric (fig. 3A). However, in HT29 cells, about half had an asymmetric shape (fig. 3C). On one side, the asymmetric asters contained a bright and concentrated microtubule bundle from which microtubules irradiated to the other side of the aster. Chromosomes were also asymmetrically distributed and were concentrated on one side of the asters, far from the bright microtubule bundles (fig. 3C). The bright microtubule bundles probably represent the duplicated centrosomes, located side by side, with chromosomes attached to the microtubules emanating from the centrosomes. In some HT29 cells, the bundle region of the asymmetric aster contained two distinct bright dots, which may represent the two partially separated centrosomes (data not shown). To rule out the possibility that asymmetric aster formation in HT29 cells was a result of a low intracellular monastrol concentration, we examined monoaster morphology as a function of monastrol concentration in the range 20–150 µM. While in HT29 cells, asymmetric monoasters appeared at all monastrol concentrations, in AGS cells we did not detect any asymmetric asters. Moreover, after 24 h of monastrol treatment, the percentage of cells with monoastral spindles was similar in both cell lines, which may indicate that the intracellular monastrol concentrations were also similar.

The kinetics of spindle recovery after release from 24 h monastrol arrest were also different in AGS and HT29 cells. The monoastral spindles disappeared more slowly in AGS than in HT29 cells. Ninety min following release, more that 10% of total AGS cells exhibited monoastral spindles, while in HT29 cells, within 40 minutes following release, less than 10% of the cells had monoastral structures (data not shown). This finding is consistent with the higher sensitivity of AGS cells to monastrol.

Taxol and monastrol induce apoptosis in AGS and HT29 cells

We found that upon treatment with taxol and monastrol, the number of cells with sub-G1 DNA content increased, indicating that they may have undergone apoptosis. Since

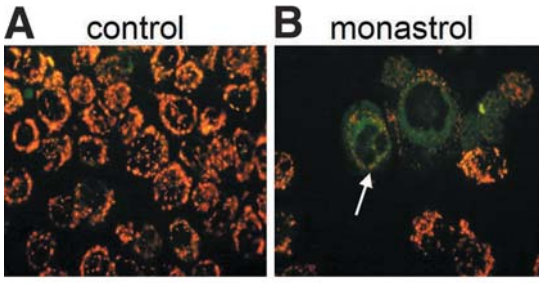

Figure 4. Mitochondrial membrane depolarization in monastrol-treated AGS cells. Mitochondrial membrane depolarization was detected by JC-1 staining of AGS cells, untreated (*A*) and treated (*B*) with 100 µM monastrol, for 24 h. Orange fluorescence is indicative of normal mitochondria and green cytoplasmic fluorescence (arrow) of depolarized mitochondria.

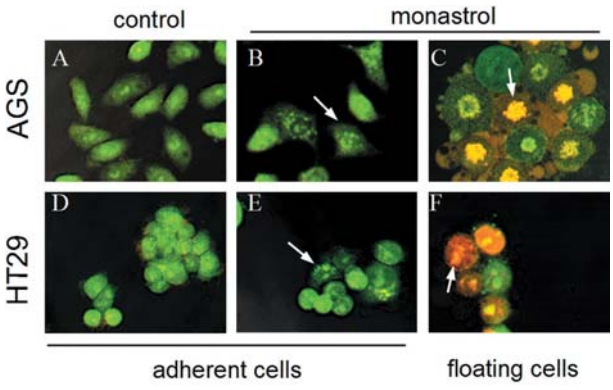

Figure 5. Acridine orange and ethidium bromide staining of early and late apoptotic AGS (*A*–*C*) and HT29 (*D*–*F*) cells, following treatment with monastrol. The stained cells were divided into the following categories [37]: green normal DNA appearance in live cells (*A*, *D*), green fragmented DNA in cells found in early apoptosis (*B*, *E*) (arrows) and orange DNA staining in cells found in late apoptosis (*C*, *F*) (arrows). The monastrol concentration was 100 µM for AGS and 150 µM for HT29 cells.

mitochondrial depolarization is one of the first stages in the apoptotic pathway, we studied the effect of monastrol on mitochondrial depolarization using the fluorescent and mitochondrial potential-sensitive dye, JC-1 [39]. In untreated samples, the majority of cells exhibited orange mitochondrial staining (fig. 4A), which indicates that mitochondrial membrane polarization was normal. On the other hand, in cells treated with monastrol, there was increased JC-1 green fluorescence (fig. 4B), representing depolarized mitochondria in early apoptotic cells. Quantification of this effect on 200 cells in four different experiments revealed that in untreated AGS cells, 4.0 ± 1.5% of cells had depolarized mitochondria, while in 24 h monastrol-treated cells, this percentage increased to 23.0 ± 4.1%. In untreated HT29 cells, 9.0 ± 4.9% of cells had depolarized mitochondria. Following 24 h of monastrol treatment, this percentage increased to 26.0 ± 7.0%. The increase in the number of cells with depolarized mitochondria following monastrol treatment in AGS and HT29 cells indicates that monastrol induces early apoptosis through mitochondrial depolarization in both cell lines.

To quantify the occurrence of early and late apoptosis, cells were subjected to acridine orange and ethidium bromide staining, which detects DNA fragmentation and loss of membrane integrity [37]. The stained cells had the following characteristics: nonapoptotic cells had a green nuclear DNA appearance (fig. 5A, D); early apoptotic cells had a green patched or fragmented DNA appearance (fig. 5B, E) and late apoptotic cells had an orange DNA appearance (fig. 5C, F). In AGS cells, after 48 h, the effect of both monastrol and taxol was similar since about 40% of the cells were found in early apoptosis and 10% in late apoptosis (fig. 6A, B). In HT29 cells, 48 h monastrol treatment induced apoptosis in only 20% of the cells (fig. 6C), while following 48 h taxol treatment, about 35% of HT29 cells underwent apoptosis (fig. 6D). These results further support our finding that AGS cells are more sensitive than HT29 cells to monastrol.

To investigate whether taxol and monastrol trigger similar apoptotic pathways, we examined the expression of the proteins procaspase 8, procaspase 3 and PARP-1 after 48 h treatment with both monastrol and taxol (fig. 7). Activation of caspases 8 and 3 was indicated by a decrease in the expression of procaspase 8 and 3, while cleavage of PARP-1 was indicated by reduced expression of the PARP-1 protein (M_r 116 kDa), and increased expression of one of its proteolytic products, p89 (fig. 7A) [40]. In AGS cells, both monastrol and taxol induced changes in the expression of these proteins. However, the activation of caspase 8 and PARP-1 cleavage were more significant after monastrol treatment (fig. 7A, B, left panels). On the other hand, in HT29 cells, activation of caspases 3 and 8, and PARP-1 cleavage were considerably more significant after taxol treatment. While taxol treatment induced a 50–75% reduction in expression of procaspase 8, 3 and PARP-1 (p116), after monastrol treatment, the reduction in expression was only up to 20% (fig. 7A, B, right panels). These results further indicate that HT29 cells are more sensitive to taxol than monastrol and that monastrol and taxol may trigger different apoptotic pathways in AGS and HT29 cells.

HsEg5 expression in AGS and HT29 cells

Since monastrol specifically inhibits the mitotic kinesin HsEg5, we examined whether differences in HsEg5 mRNA expression could account for the differences in sensitivity to monastrol of AGS and HT29 cells. For this purpose, cells were treated with monastrol or taxol, and HsEg5 mRNA levels, relative to β-actin mRNA levels, were determined by PCR and real-time RT-PCR analysis (fig. 8). In control and monastrol-treated HT29 cells, relative HsEg5 expression was about 1.5-fold higher than in control and monastrol-treated AGS cells (fig. 8B) and in

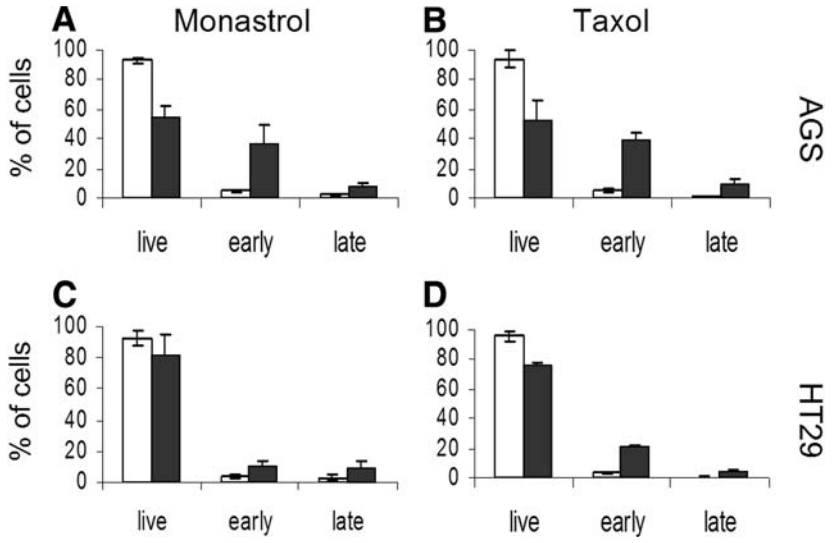

Figure 6. Early and late apoptosis induction by monastrol and taxol in AGS and HT29 cells. Cells treated with monastrol (*A*, *C*) and taxol (*B*, *D*) [AGS (*A*, *B*) and HT29 (*C*, *D*)] for 48 h were stained with acridine orange and ethidium bromide to quantify early and late apoptosis. White columns represent control cells, while black columns represent monastrol- or taxol-treated cells. In each experiment, 200 cells were counted and categorized as described in figure 5. The percentage of cells in each category is indicated. Columns and bars represent averages and SDs of four experiments.

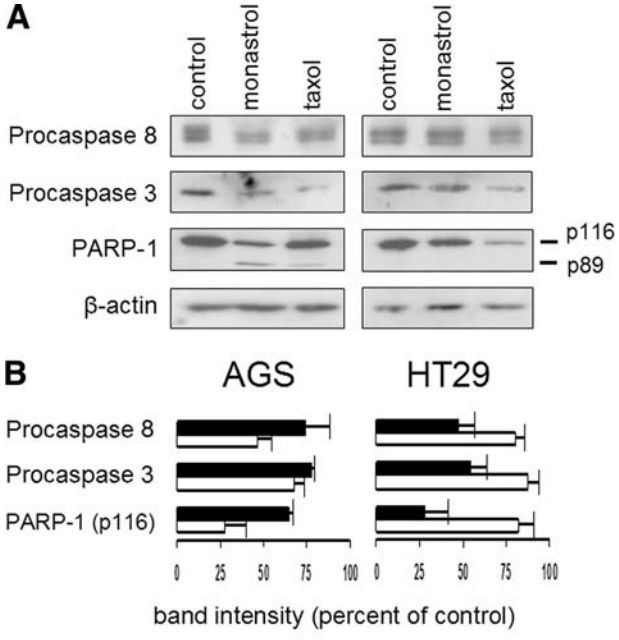

Figure 7. Expression of procaspase 8, procaspase 3, PARP-1 and β-actin was followed by Western blot analysis in AGS cells (left) and HT29 cells (right) treated for 48 h with monastrol or taxol (*A*), and procaspase 8, 3 and PARP-1 (p116) expression after treatment with monastrol (white) and taxol (black) were quantified (*B*). See Materials and methods for description. Results are averages and SD of three or four independent experiments.

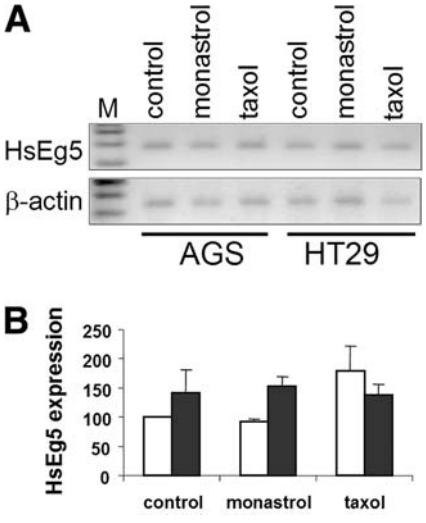

Figure 8. HsEg5 mRNA expression in AGS and HT29 cells, treated with monastrol and taxol for 24 h. (*A*) Representative results of RT-PCR and β-actin products fractionated on 2% agarose gel. Treatment conditions are indicated at the top of the panel and the cell type at the bottom of the panel; M, molecular-weight markers. (*B*) Real-time RT-PCR analysis of relative HsEg5 expression in AGS (white columns) and HT29 (black columns) cells, normalized to expression in AGS control samples. Columns and bars represent average and SD of three independent experiments. Taxol concentration, 10 nM; monastrol concentrations, 100 µM for AGS and 150 µM for HT29 cells.

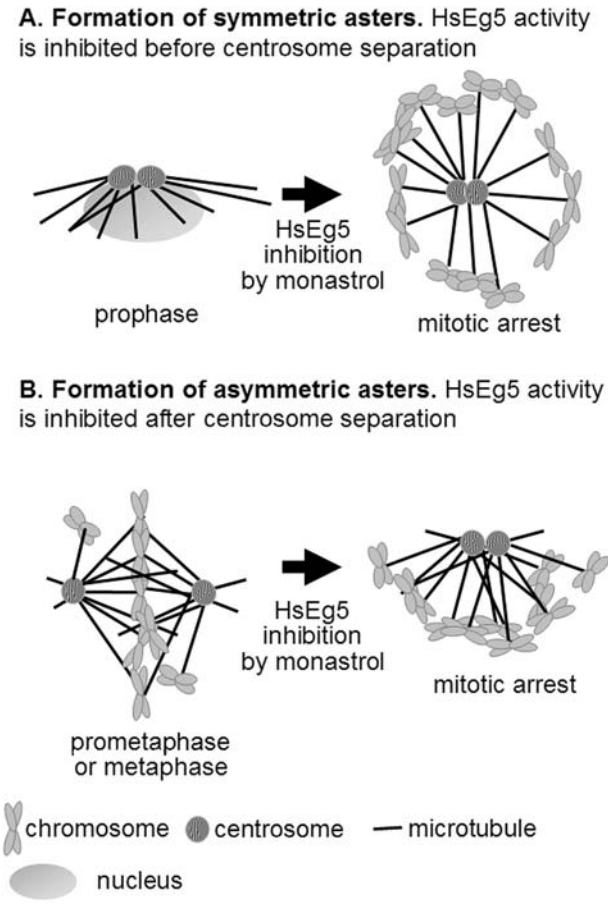

Figure 9. Possible mechanisms for the formation of symmetric and asymmetric asters in HT29 cells. (*A*) HsEg5 activity is inhibited by monastrol before centrosome separation, which results in the formation of symmetric microtubule asters. (*B*) HsEg5 activity is inhibited after centrosome separation or spindle formation, which may result in the formation of asymmetric asters with centrosomes on one side, microtubules emanating from the centrosomes, and chromosomes attached to the microtubule ends far from the centrosomes.

both cell lines, HsEg5 expression was not altered by monastrol treatment. On the other hand, in AGS cells, incubation with taxol increased HsEg5 by 1.8 ± 0.4-fold. In HT29 cells, taxol did not affect the relative expression levels of HsEg5. These results indicate that in control and monastrol-treated samples, HT29 cells which are less sensitive to monastrol, express slightly higher levels of HsEg5 mRNA compared to the more sensitive AGS cells. However, whether such small differences in HsEg5 mRNA expression can account for the profound differences in sensitivity to monastrol of the two cell lines is questionable.

Discussion

One of the important features of monastrol is that it can be used to evaluate whether a specific inhibitor of HsEg5 can be used as an anticancer agent. However, to develop in vitro assays for prediction of tumor sensitivity to monastrol, the long-term effects of monastrol on several human cell types need to be characterized. This is the first study to investigate the long-term effects of monastrol on two human cell lines, AGS from gastric carcinoma and HT29 from colon carcinoma. We found that the two cell types responded differently to monastrol, HT29 cells being considerably less sensitive than AGS cells. The differences between the cell lines were determined by the degree of the inhibitory effect on cell proliferation (fig. 1), reversibility of monastrol-induced mitotic arrest (fig. 2), intracellular microtubule phenotypes (fig. 3), kinetics of the release from monastrol-induced mitotic arrest and induction of apoptosis (figs 6, 7).

The molecular mechanisms which can explain the differences in sensitivity to monastrol are not yet clear. Since the two examined cell lines are not isogenic, multiple factors could account for these differences. For example, HT29 but not AGS cells are mutated in the p53 transcription factor which was recently implicated to play a role in the spindle checkpoint through regulation of the Polo-like kinase Snk/Plk2 [41]. Although mutated p53 was suggested to increase sensitivity to taxol [42, 43], it can function in an opposite manner with respect to monastrol, since the two drugs impose mitotic arrest by different mechanisms. Another possible candidate for mediating the effects of monastrol is the c-myc transcription factor [44]. Overexpression of c-myc was shown to attenuate irradiation-imposed G2/M arrest [45] and to modulate cellular responses to taxol [46]. Moreover, c-myc directly interacts with α-tubulin and microtubules [47, 48]. Finally, c-myc expression is affected by drugs which alter microtubule dynamics [48, 49]. We found by real-time PCR analysis that c-myc mRNA expression relative to β-actin is about twofold higher in HT29 than in AGS cells (data not shown). Since c-myc is involved in numerous intracellular regulatory cascades [for reviews see refs 50, 51], this difference in c-myc expression may account, at least in part, for the difference in sensitivity to monastrol. In any event, although HT29 cells express higher mRNA levels of the monastrol target protein HsEg5 (fig. 8B), this difference is rather small, 1.5-fold, and probably does not account for the differential effects of monastrol on these two cell lines. More studies on these and additional cell lines are required to fully characterize the effects of monastrol on human cells and to establish the cause for the different sensitivity to the drug.

Asymmetric aster formation

We demonstrated that in human HT29 cells, in addition to the originally reported monastrol-induced microtubule phenotype, the symmetric monoaster [9, 10, 13] (fig. 3A, B), other monastrol-induced microtubule arrangements, such as asymmetric asters or monopolar spindles (fig.

3C) also exist. In mammalian cell lines from rat kangaroo *Potorous tridactylis* kidney epithelium, monastrol induces monopolar spindle formation in a majority of cells [10, 36]. The number of chromosomes in rat kangaroo cells is very small (2n = 12–13) but their size is large, compared to other mammalian species. Monastrol-induced monopolar spindle formation in rat kangaroo cells may be directly related to these factors. Another possibility is that monopolar spindle formation is related to specific spindle dynamics mechanisms. Interestingly, asymmetric asters were also observed in human HeLa cells injected with anti-Eg5 antibodies [21]. Although the percentage of HeLa cells with asymmetric asters was not quantified [21], this finding suggests that inhibition of the HsEg5 function can result in the formation of asymmetric asters in some human cell types.

The formation of the asymmetric asters in HT29 cells is unlikely to result from a low intracellular monastrol concentration, since 150 µM monastrol efficiently inhibited cell proliferation and induced G2/M cell cycle arrest (figs 1, 2). In addition, in AGS cells, asymmetric monoasters were not observed, even when cells were treated with low, 20 µM monastrol, for 24 h, or with 100 µM monastrol for shorter periods (data not shown). Finally, BS-C-1 cells treated with monastrol for only 4 h produced no asymmetric asters [10], which indicates that the formation of asymmetric asters may reflect a specific mechanism(s) by which HsEg5 participates in spindle dynamics in HT29 cells.

A possible explanation for the formation of asymmetric asters in HT29 cells is that HsEg5 function is inhibited by monastrol after centrosomes are separated or mitotic spindles are formed (fig. 9). When centrosomes are separated, microtubules emanating from different centrosomes are cross-linked by HsEg5 activity. Then, once the HsEg5 function is inhibited by monastrol, the spindles collapse and the centrosomes are drawn together by an inwardly directed force, probably provided by the KAR3 human homologue, HSET [52]. This creates asymmetric microtubule arrays with the two centrosomes located close together on one side, microtubules emanating from these centrosomes and chromosomes attached to the microtubules (fig. 9). If mitotic spindles are formed prior to monastrol inhibition of HsEg5 function, the chromosomes will attach to kinetochore microtubules emanating from opposite spindle poles. This attachment contributes to the asymmetry of the collapsed spindles, since kinetochore attachment to microtubules is not inhibited by monastrol [10]. A similar spindle collapse was reported in *Saccharomyces cerevisiae* cells in which BimC function was eliminated after the formation of the mitotic spindle [53]. This experiment demonstrated that in *S. cerevisiae* cells, the BimC motor function is required both before and after spindle assembly. Therefore, formation of asymmetric asters in HT29 cell lines (fig. 3C) may indicate the importance of HsEg5 function after spindle formation as well.

Induction of apoptosis

Previous studies have demonstrated that elimination of BimC function causes mitotic cell cycle arrest which eventually leads to cell death [21, 54]. However, the exact mechanisms have not as yet been studied. We demonstrated that in both AGS and HT29 cells, mitotic arrest induced by both monastrol and taxol leads to cell death by the apoptotic pathway (figs 4–7). In agreement with the lower sensitivity of HT29 cells to monastrol, apoptosis was less pronounced in these cells, although HT29 cells were treated with a higher monastrol concentration (150 µM) than were AGS cells (100 µM). The lower sensitivity of HT29 cells to monastrol was demonstrated by acridine orange and ethidium bromide staining (fig. 6), by considerably reduced caspase 8 and 3 activation and a smaller degree of PARP-1 cleavage (fig. 7). The reduced degree of apoptosis induction in HT29 cells is specific to monastrol since treatment with taxol induced significant apoptosis (figs. 6, 7). Mitotic arrest has been suggested to also induce differentiation [55]. By examining alkaline phosphatase activity, we found that differentiation does not occur as a function of prolonged monastrol treatment of HT29 cells (data not shown). Why HT29 cells are more resistant to monastrol-induced apoptosis is not clear. However, the resistance to apoptosis (figs. 6, 7) and reversibility of prolonged monastrol-induced arrest (fig. 2B) demonstrated here for HT29 cells can occur also in cancer tissue and are undesired effects from a therapeutic perspective.

Mitotic arrest induced by taxol has been shown to lead to apoptosis via mitochondrial membrane depolarization [31, 33, 56, 57]. In the present study, we directly demonstrated by JC-1 staining that mitochondrial depolarization also occurs in AGS and HT29 cells arrested in mitosis by monastrol (fig. 4 and text). However, the caspase activation pathways that follow mitochondrial membrane depolarization may vary in the two cell lines. In AGS cells, monastrol-induced mitochondrial membrane depolarization was accompanied by caspase 8 and 3 activation and PARP-1 cleavage, while in HT29 cells, caspase 3 and 8 activation and PARP-1 cleavage were minimal (fig. 7). Since in monastrol-treated HT29 cells, apoptosis was detected by both JC-1 and acridine orange and ethidium bromide staining, in HT29 cells, other intracellular pathways may be involved in monastrol-induced apoptosis. Although the percentage of apoptotic cells was similar in AGS cells after treatment with both monastrol and taxol (fig. 6A, B), the activation of caspase 8 and PARP-1 cleavage was more significant after monastrol treatment (fig. 7B). This may indicate that additional apoptotic pathways are activated by taxol in AGS cells. Finally, while the effect of taxol was similar in the two cell lines

(figs 1B, 6B, D), caspase 8, 3 and PARP-1 cleavage after taxol treatment were more pronounced in HT29 than in AGS cells (fig. 7B). Monastrol and taxol induce mitotic arrest by disrupting the spindle by different mechanisms. While taxol stabilizes microtubules, monastrol inhibits HsEg5 activity without affecting microtubule dynamics. Based on our results we conclude that these different mechanisms trigger different apoptotic pathways that may be cell type specific.

Acknowledgements. This research was supported in part by grant no. 339/00 from The Israeli Science Foundation – The Charles H. Revson Foundation and by grant no. 9049/01 from The Israeli Science Foundation.

1 Hildebrandt E. R. and Hoyt M. A. (2000) Mitotic motors in *Saccharomyces cerevisiae*. Biochim. Biophys. Acta **1496:** 99–116
2 Cleveland D. W., Mao Y. and Sullivan K. F. (2003) Centromeres and kinetochores: from epigenetics to mitotic checkpoint signaling. Cell **112:** 407–421
3 Kapoor T. M. and Compton D. A. (2002) Searching for the middle ground: mechanisms of chromosome alignment during mitosis. J. Cell Biol. **157:** 551–556
4 Scholey J. M., Brust-Mascher I. and Mogilner A. (2003) Cell division. Nature **422:** 746–752
5 Chen J. G. and Horwitz S. B. (2002) Differential mitotic responses to microtubule-stabilizing and -destabilizing drugs. Cancer Res. **62:** 1935–1938
6 Green M. C. and Hortobagyi G. N. (2002) Adjuvant chemotherapy for breast cancer. Langenbecks Arch. Surg. **387:** 109–116
7 Mukherjee A. K., Basu S., Sarkar N. and Ghosh A. C. (2001) Advances in cancer therapy with plant based natural products. Curr. Med. Chem. **8:** 1467–1486
8 Tang C., Willingham M. C., Reed J. C., Miyashita T., Ray S., Ponnathpur V. et al. (1994) High levels of p26BCL-2 oncoprotein retard taxol-induced apoptosis in human pre-B leukemia cells. Leukemia **8:** 1960–1969
9 Mayer T. U., Kapoor T. M., Haggarty S. J., King R. W., Schreiber S. L. and Mitchison T. J. (1999) Small molecule inhibitor of mitotic spindle bipolarity identified in a phenotype-based screen. Science **286:** 971–974
10 Kapoor T. M., Mayer T. U., Coughlin M. L. and Mitchison T. J. (2000) Probing spindle assembly mechanisms with monastrol, a small molecule inhibitor of the mitotic kinesin, Eg5. J. Cell Biol. **150:** 975–988
11 Kapoor T. M. and Mitchison T. J. (2001) Eg5 is static in bipolar spindles relative to tubulin: evidence for a static spindle matrix. J. Cell Biol. **154:** 1125–1133
12 Maliga Z., Kapoor T. M. and Mitchison T. J. (2002) Evidence that monastrol is an allosteric inhibitor of the mitotic kinesin Eg5. Chem. Biol. **9:** 989–996
13 DeBonis S., Simorre J. P., Crevel I., Lebeau L., Skoufias D. A., Blangy A. et al. (2003) Interaction of the mitotic inhibitor monastrol with human kinesin Eg5. Biochemistry **42:** 338–349
14 Enos A. P. and Morris N. R. (1990) Mutation of a gene that encodes a kinesin-like protein blocks nuclear division in *A. nidulans*. Cell **60:** 1019–1027
15 Hoyt M. A., He L., Loo K. K. and Saunders W. S. (1992) Two *Saccharomyces cerevisiae* kinesin-related gene products required for mitotic spindle assembly. J. Cell Biol. **118:** 109–120
16 Roof D. M., Meluh P. B. and Rose M. D. (1992) Kinesin-related proteins required for assembly of the mitotic spindle. J. Cell Biol. **118:** 95–108
17 Hagan I. and Yanagida M. (1992) Kinesin-related cut7 protein associates with mitotic and meiotic spindles in fission yeast. Nature **356:** 74–76
18 Heck M. M., Pereira A., Pesavento P., Yannoni Y., Spradling A. C. and Goldstein L. S. (1993) The kinesin-like protein KLP61F is essential for mitosis in *Drosophila*. J. Cell Biol. **123:** 665–679
19 Le Guellec R., Paris J., Couturier A., Roghi C. and Philippe M. (1991) Cloning by differential screening of a *Xenopus* cDNA that encodes a kinesin-related protein. Mol. Cell. Biol. **11:** 3395–3398
20 Asada T., Kuriyama R. and Shibaoka H. (1997) TKRP125, a kinesin-related protein involved in the centrosome-independent organization of the cytokinetic apparatus in tobacco BY-2 cells. J. Cell Sci. **110:** 179–189
21 Blangy A., Lane H. A., d'Herin P., Harper M., Kress M. and Nigg E. A. (1995) Phosphorylation by p34cdc2 regulates spindle association of human Eg5, a kinesin-related motor essential for bipolar spindle formation in vivo. Cell **83:** 1159–1169
22 Kashina A. S., Rogers G. C. and Scholey J. M. (1997) The bimC family of kinesins: essential bipolar mitotic motors driving centrosome separation. Biochim. Biophys. Acta **1357:** 257–271
23 Walczak C. E. and Mitchison T. J. (1996) Kinesin-related proteins at mitotic spindle poles: function and regulation. Cell **85:** 943–946
24 Gheber L., Kuo S. C. and Hoyt M. A. (1999) Motile properties of the kinesin-related Cin8p spindle motor extracted from *Saccharomyces cerevisiae* cells. J. Biol. Chem. **274:** 9564–9572
25 Kerr J. F., Wyllie A. H. and Currie A. R. (1972) Apoptosis: a basic biological phenomenon with wide-ranging implications in tissue kinetics. Br. J. Cancer **26:** 239–257
26 Arends M. J., Morris R. G. and Wyllie A. H. (1990) Apoptosis: the role of the endonuclease. Am. J. Pathol. **136:** 593–608
27 Patel T., Gores G. J. and Kaufmann S. H. (1996) The role of proteases during apoptosis. FASEB J. **10:** 587–597
28 Soldani C. and Scovassi A. I. (2002) Poly(ADP-ribose) polymerase-1 cleavage during apoptosis: an update. Apoptosis **7:** 321–328
29 Inoue S., Salah-Eldin A. E. and Omoteyama K. (2001) Apoptosis and anticancer drug resistance. Hum. Cell **14:** 211–221
30 Cohen E., Ophir I. and Shaul Y. B. (1999) Induced differentiation in HT29, a human colon adenocarcinoma cell line. J. Cell Sci **112:** 2657–2666
31 Goncalves A., Braguer D., Carles G., Andre N., Prevot C. and Briand C. (2000) Caspase-8 activation independent of CD95/CD95-L interaction during paclitaxel-induced apoptosis in human colon cancer cells (HT29-D4). Biochem. Pharmacol. **60:** 1579–1584
32 Oyaizu H., Adachi Y., Taketani S., Tokunaga R., Fukuhara S. and Ikehara S. (1999) A crucial role of caspase 3 and caspase 8 in paclitaxel-induced apoptosis. Mol. Cell. Biol. Res. Commun. **2:** 36–41
33 Yuan S. Y., Hsu S. L., Tsai K. J. and Yang C. R. (2002) Involvement of mitochondrial pathway in taxol-induced apoptosis of human T24 bladder cancer cells. Urol. Res. **30:** 282–288
34 Yang C. P. and Horwitz S. B. (2002) Distinct mechanisms of taxol-induced serine phosphorylation of the 66-kDa Shc isoform in A549 and RAW 264.7 cells. Biochim. Biophys. Acta **1590:** 76–83
35 Ibrado A. M., Huang Y., Fang G. and Bhalla K. (1996) Bcl-xL overexpression inhibits taxol-induced Yama protease activity and apoptosis. Cell Growth. Differ. **7:** 1087–1094
36 Canman J. C., Cameron L. A., Maddox P. S., Straight A., Tirnauer J. S., Mitchison T. J. et al. (2003) Determining the position of the cell division plane. Nature **424:** 1074–1078
37 McGahon A. J., Martin S. J., Bissonnette R. P., Mahboubi A., Shi Y., Mogil R. J. et al. (1995) The end of the (cell) line: methods for the study of apoptosis in vitro. Methods Cell Biol. **46:** 153–185

38 Abal M., Andreu J. M. and Barasoain I. (2003) Taxanes: microtubule and centrosome targets, and cell cycle dependent mechanisms of action. Curr. Cancer Drug Targets **3:** 193–203
39 Cossarizza A., Baccarani-Contri M., Kalashnikova G. and Franceschi C. (1993) A new method for the cytofluorimetric analysis of mitochondrial membrane potential using the J-aggregate forming lipophilic cation 5,5′,6,6′-tetrachloro-1,1′, 3,3′-tetraethylbenzimidazolcarbocyanine iodide (JC-1). Biochem. Biophys. Res. Commun. **197:** 40–45
40 Decker P. and Muller S. (2002) Modulating poly (ADP-ribose) polymerase activity: potential for the prevention and therapy of pathogenic situations involving DNA damage and oxidative stress. Curr. Pharm. Biotechnol. **3:** 275–283
41 Burns T. F., Fei P., Scata K. A., Dicker D. T. and El-Deiry W. S. (2003) Silencing of the novel p53 target gene Snk/Plk2 leads to mitotic catastrophe in paclitaxel (taxol)-exposed cells. Mol. Cell. Biol. **23:** 5556–5571
42 Wahl A. F., Donaldson K. L., Fairchild C., Lee F. Y., Foster S. A., Demers G. W. et al. (1996) Loss of normal p53 function confers sensitization to taxol by increasing G2/M arrest and apoptosis. Nat. Med. **2:** 72–79
43 Vikhanskaya F., Vignati S., Beccaglia P., Ottoboni C., Russo P., D'Incalci M. et al. (1998) Inactivation of p53 in a human ovarian cancer cell line increases the sensitivity to paclitaxel by inducing G2/M arrest and apoptosis. Exp. Cell Res. **241:** 96–101
44 Prochownik E. V. (2004) c-Myc as a therapeutic target in cancer. Expert Rev. Anticancer. Ther. **4:** 289–302
45 Sheen J. H., Woo J. K. and Dickson R. B. (2003) c-Myc alters the DNA damage-induced G2/M arrest in human mammary epithelial cells. Br. J. Cancer **89:** 1479–1485
46 Bottone M. G., Soldani C., Tognon G., Gorrini C., Lazze M. C., Brison O. et al. (2003) Multiple effects of paclitaxel are modulated by a high c-myc amplification level. Exp. Cell Res. **290:** 49–59
47 Alexandrova N., Niklinski J., Bliskovsky V., Otterson G. A., Blake M., Kaye F. J. et al. (1995) The N-terminal domain of c-Myc associates with alpha-tubulin and microtubules in vivo and in vitro. Mol. Cell. Biol. **15:** 5188–5195
48 El Khyari S., Bourgarel V., Barra Y., Braguer D. and Briand C. (1997) Pretreatment by tubulin agents decreases C-MYC induction in human colon carcinoma cell line HT29-D4. Biochem. Biophys. Res. Commun. **231:** 751–754
49 Bourgarel-Rey V., El Khyari S., Rimet O., Bordas B., Guigal N., Braguer D. et al. (2000) Opposite effects of antimicrotubule agents on c-myc oncogene expression depending on the cell lines used. Eur. J. Cancer **36:** 1043–1049
50 Nilsson J. A., Cleveland J. L. and Kikuchi A. (2003) Myc pathways provoking cell suicide and cancer: regulation of beta-catenin signaling in the Wnt pathway. Oncogene **22:** 9007–9021
51 Kikuchi A. (2000) Regulation of beta-catenin signaling in the Wnt pathway. Biochem. Biophys. Res. Commun. **268:** 243–248
52 Mountain V., Simerly C., Howard L., Ando A., Schatten G. and Compton D. A. (1999) The kinesin-related protein, HSET, opposes the activity of Eg5 and cross-links microtubules in the mammalian mitotic spindle. J. Cell Biol. **147:** 351–366
53 Saunders W. S. and Hoyt M. A. (1992) Kinesin-related proteins required for structural integrity of the mitotic spindle. Cell **70:** 451–458
54 Hoyt M. A., Totis L. and Roberts B. T. (1991) *S. cerevisiae* genes required for cell cycle arrest in response to loss of microtubule function. Cell **66:** 507–517
55 Banerjee S., Fallis A. G. and Brown D. L. (1997) Differential effects of taxol on two human cancer cell lines. Oncol. Res. **9:** 237–248
56 Haefen C. von, Wieder T., Essmann F., Schulze-Osthoff K., Dorken B. and Daniel P. T. (2003) Paclitaxel-induced apoptosis in BJAB cells proceeds via a death receptor-independent, caspases-3/-8-driven mitochondrial amplification loop. Oncogene **22:** 2236–2247
57 Wieder T., Essmann F., Prokop A., Schmelz K., Schulze-Osthoff K., Beyaert R. et al. (2001) Activation of caspase-8 in drug-induced apoptosis of B-lymphoid cells is independent of CD95/Fas receptor-ligand interaction and occurs downstream of caspase-3. Blood **97:** 1378–1387